Electronic Supplemental Information for

Computational screening and mechanistic insights of oxygen-terminated MOenes for electrocatalytic hydrogen evolution†

Meng Tian*

School of New Energy, Nanjing University of Science and Technology, Jiangyin 214443, Jiangsu, China

*Corresponding author: tianmeng@njust.edu.cn

Computational details

Density functional theory (DFT) calculations were performed using the Vienna *ab initio* simulation package (VASP).[1] Perdew-Burke-Ernzerhof functional (PBE) with the generalized gradient approximation was adopted to compute the exchange-correction functional.[2] Valence electron configurations of the pseudopotentials were set as $3p^6 3d^1 4s^2$ for Sc, $3d^2 4s^2$ for Ti, $3p^6 3d^3 4s^2$ for V, $3d^5 4s^1$ for Cr, $4s^2 4p^6 4d^1 5s^2$ for Y, $4s^2 4p^6 4d^2 5s^2$ for Zr, $4p^6 4d^4 5s^1$ for Nb, $4p^6 4d^5 5s^1$ for Mo, $5d^2 6s^2$ for Hf, $5d^3 6s^2$ for Ta, $5d^4 6s^2$ for W, $2s^2 2p^4$ for O, $3s^2 3p^4$ for S, $4s^2 4p^4$ for Se, $5s^2 5p^4$ for Te, respectively. The assumed orbital angular momentum (L), spin angular momentum (S), and total angular momentum (J) are computed based on these valence electron configurations, as shown in Table S1. All MOenes models were built with a 15-Å thickness vacuum along *z*-axis. The element substitution method was employed to achieve doping strategy. The energy-correction term of van der Waals dispersion for 2D MOenes was computed with DFT + D3 method.[3] The spin-orbital coupling was considered due to the existence of transition metals. All structures were fully relaxed with cutoff energy of 500 eV, energy convergence of 10^{-5} eV, and force convergence of 0.01 eV/Å. The Monkhorst–Pack *K*-point sampling grids were 7 × 7 × 1 for unit cells, and 2 × 2 × 1 for 4 × 4 × 1 supercells, respectively. Hydrogen evolution reaction was computed based on the J. K. Nørskov model.[4] Both entropy and zero-point energy corrections were considered at 298.15 K to obtain the Gibbs free energy change, as follows:

$$\Delta G_{*H} = \Delta E_{*H} + \Delta E_{ZPE} - T\Delta S_{*H} \quad (1)$$

where ΔE_{*H}, ΔE_{ZPE}, T, and ΔS_{*H} stand for the free energy of H adsorption, zero-point energy, temperature, and entropy correction, respectively. ΔE_{*H} was computed using the following equation:

$$\Delta E_{*H} = E_{Catalyst + H} - E_{Catalyst} - 0.5*E_{H2} \quad (2)$$

where $E_{Catalyst + H}$ is the total energy of the catalyst model after H adsorption, $E_{Catalyst}$ is the total energy of the catalyst, and E_{H2} is the total energy of an isolated H_2 molecule. The term $T*\Delta S_{*H}$ primarily arises from the entropy loss of the reference state (gaseous H_2). According to ΔG_{*H}, the hydrogen evolution exchange current density (i) was computed using the following equation:

$$i = -ek_0 \frac{1}{1 + exp(\frac{|\Delta G_{*H}|}{k_B T})} \quad (3)$$

where e, k_0, and k_B represent electron, the rate constant (set as 200 s^{-1} site $^{-1}$), and Boltzmann constant, respectively.[4] The climbing-image nudged elastic band (CI-NEB) method was used to reveal the reaction mechanism of hydrogen evolution.[5] The dynamics stability was verified using the *Ab initio* molecular dynamics (AIMD) simulation at 300 K lasting 5 ps with 1 fs each step.[6] The electronic and structural analysis (VESTA) software was employed to visualize the crystal structure.[7] The nonlocal Heyd-Scuseria-Ernzerhof (HSE06) hybrid functional was employed to compute the electronic band structures of these candidates.[8]

Table S1 The valence electron, orbital angular momentum (L), spin angular momentum (S), and total angular momentum (J) for each element.

Element	Valence electron	Orbital angular momentum (L)	Spin angular momentum (S)	Total angular momentum (J)	Group level
Sc	$3p^6 3d^1 4s^2$	2	1/2	3/2	$^2D_{3/2}$
Ti	$3d^2 4s^2$	3	1	2	$^3F_2$
V	$3p^6 3d^3 4s^2$	3	3/2	3/2	$^4F_{3/2}$
Cr	$3d^5 4s^1$	0	3	3	$^7S_3$
Y	$4s^2 4p^6 4d^1 5s^2$	2	1/2	3/2	$^2D_{3/2}$
Zr	$4s^2 4p^6 4d^2 5s^2$	3	1	2	$^3F_2$
Nb	$4p^6 4d^4 5s^1$	2	5/2	1/2	$^6D_{1/2}$
Mo	$4p^6 4d^5 5s^1$	0	3	3	$^7S_3$
Hf	$5d^2 6s^2$	3	1	2	$^3F_2$
Ta	$5d^3 6s^2$	3	3/2	3/2	$^4F_{3/2}$
W	$5d^4 6s^2$	2	2	0	$^5D_0$
O	$2s^2 2p^4$	1	1	2	$^3P_2$
S	$3s^2 3p^4$	1	1	2	$^3P_2$
Se	$4s^2 4p^4$	1	1	2	$^3P_2$
Te	$5s^2 5p^4$	1	1	2	$^3P_2$

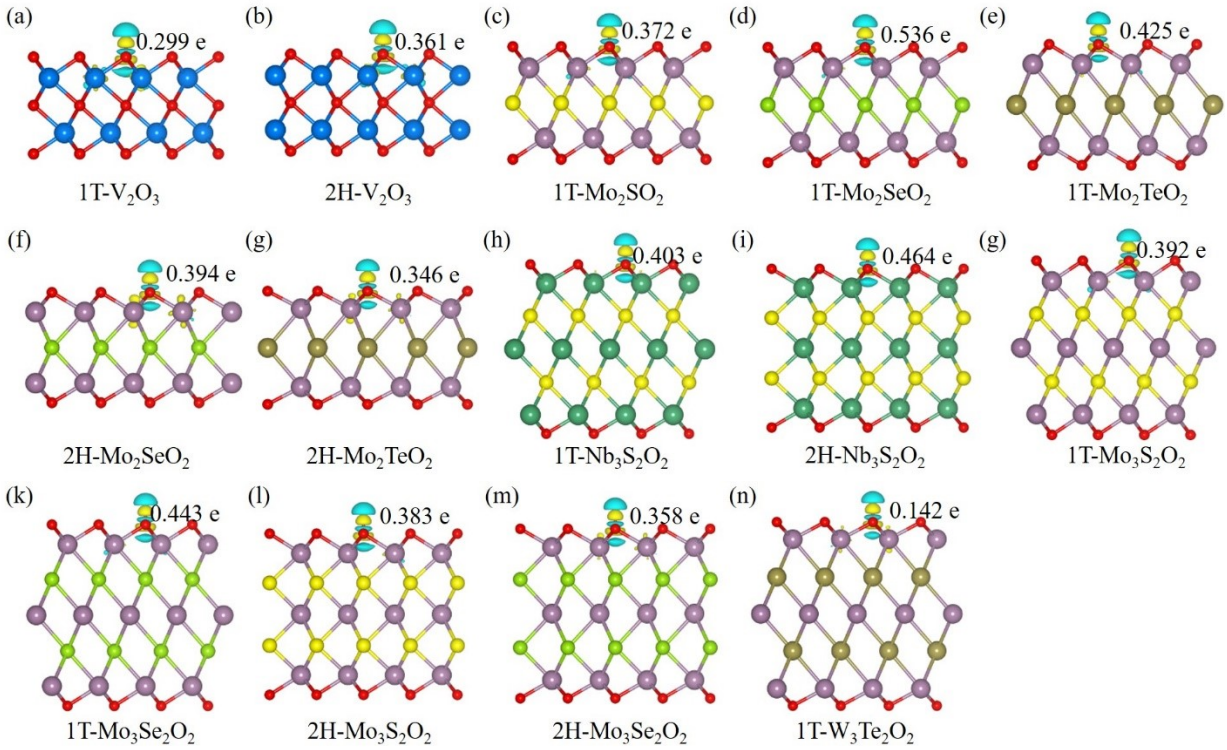

Fig. S1 Charge density difference for (a) 1T-V_2O_3, (b) 2H-V_2O_3, (c) 1T-Mo_2SO_2, (d) 1T-Mo_2SeO_2, (e) 1T-Mo_2TeO_2, (f) 2H-Mo_2SeO_2, (g) 2H-Mo_2TeO_2, (h) 1T-$Nb_3S_2O_2$, (i) 2H-$Nb_3S_2O_2$, (g) 1T-$Mo_3S_2O_2$, (k) 1T- $Mo_3Se_2O_2$, (l) 2H-$Mo_3S_2O_2$, (m) 2H- $Mo_3Se_2O_2$, and (n) 1T- $W_3Te_2O_2$, respectively.

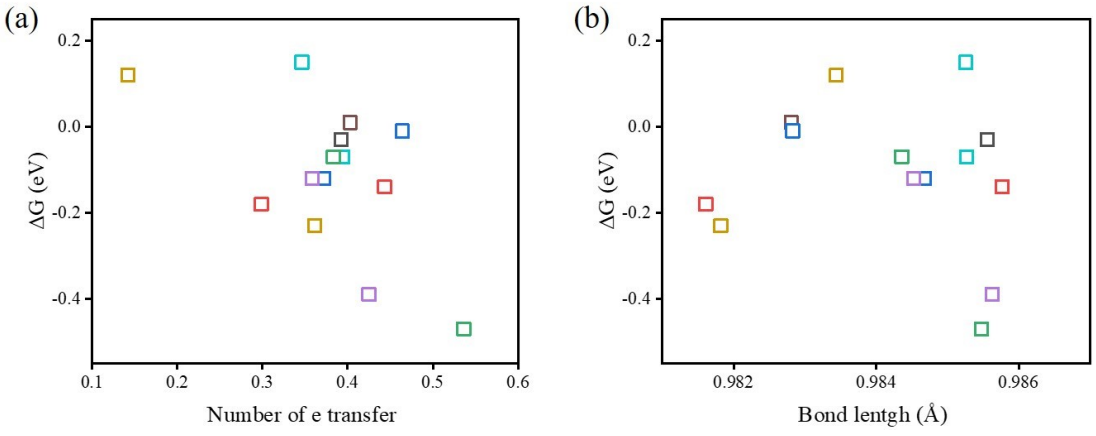

Fig. S2 (a) The relationship between ΔG_{*H} and number of electron transfer during hydrogen adsorption. (b) The relationship between ΔG_{*H} and O-H bond.

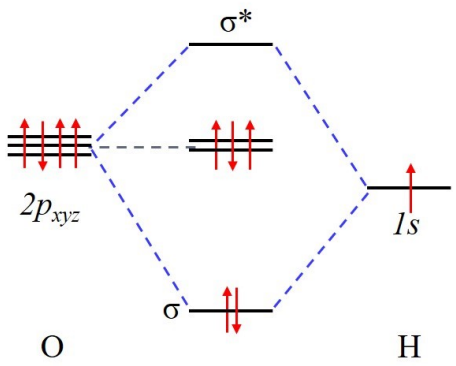

Fig. S3 The hybridization between O-2p and H-1s orbitals.

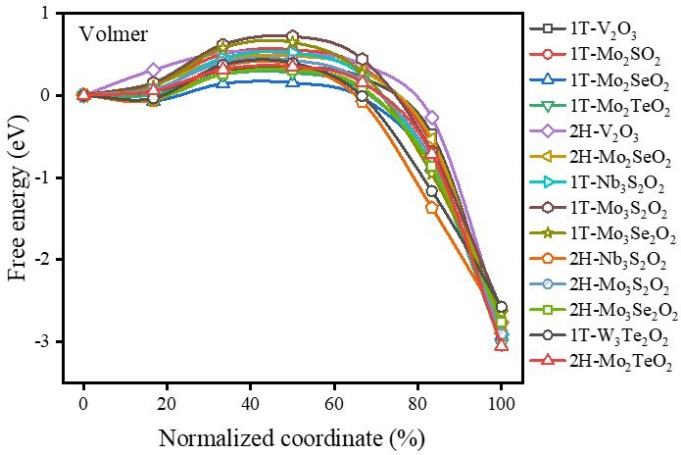

Fig. S4 The relationship between free energy and normalized pathway for Volmer reaction.

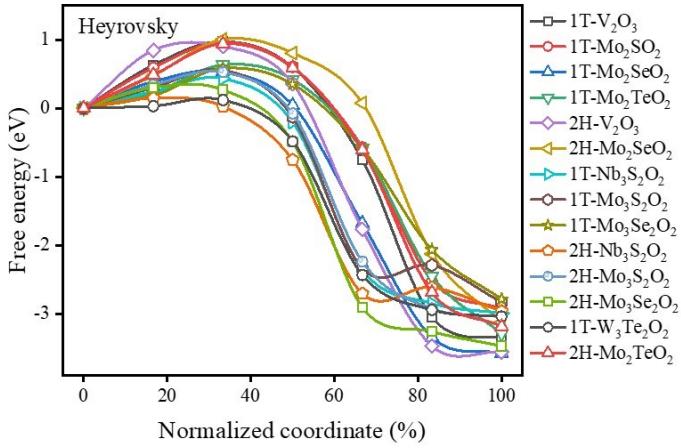

Fig. S5 The relationship between free energy and normalized pathway for Heyrovsky reaction.

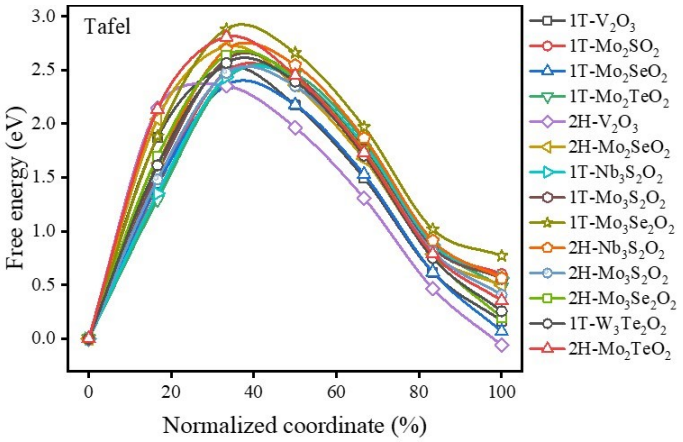

Fig. S6 The relationship between free energy and normalized pathway for Tafel reaction.

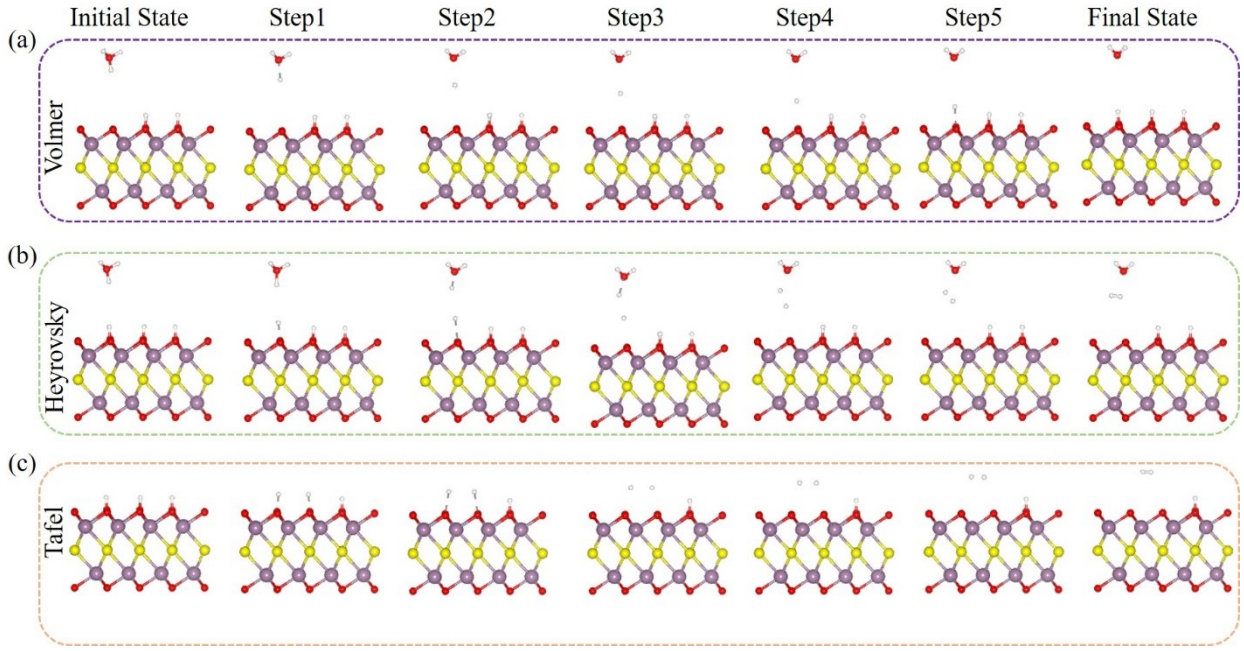

Fig. S7 Schematic structures for (a) Volmer, (b) Heyrovsky, and (c) Tafel reactions from CINEB calculations, respectively.

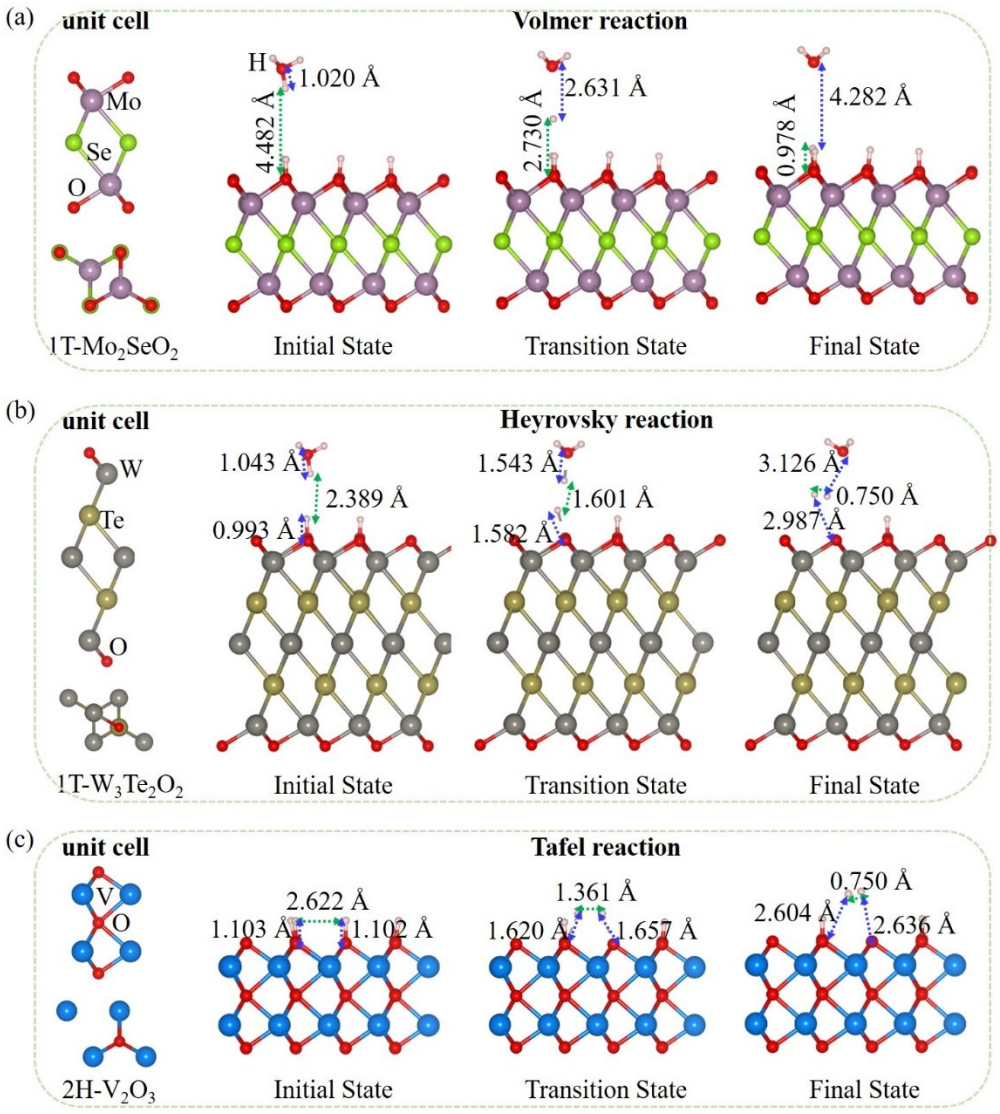

Fig. S8 The accurate geometries for each of the most favorable cases (a) 1T-Mo_2SeO_2 for Volmer reaction, (b) 1T-$W_3Te_2O_2$ for Heyrovsky reaction, and (c) 2H-V_2O_3 for Tafel reaction. The left is the unit cell for each chemical composition. The distances for O–H and H–H are provided.

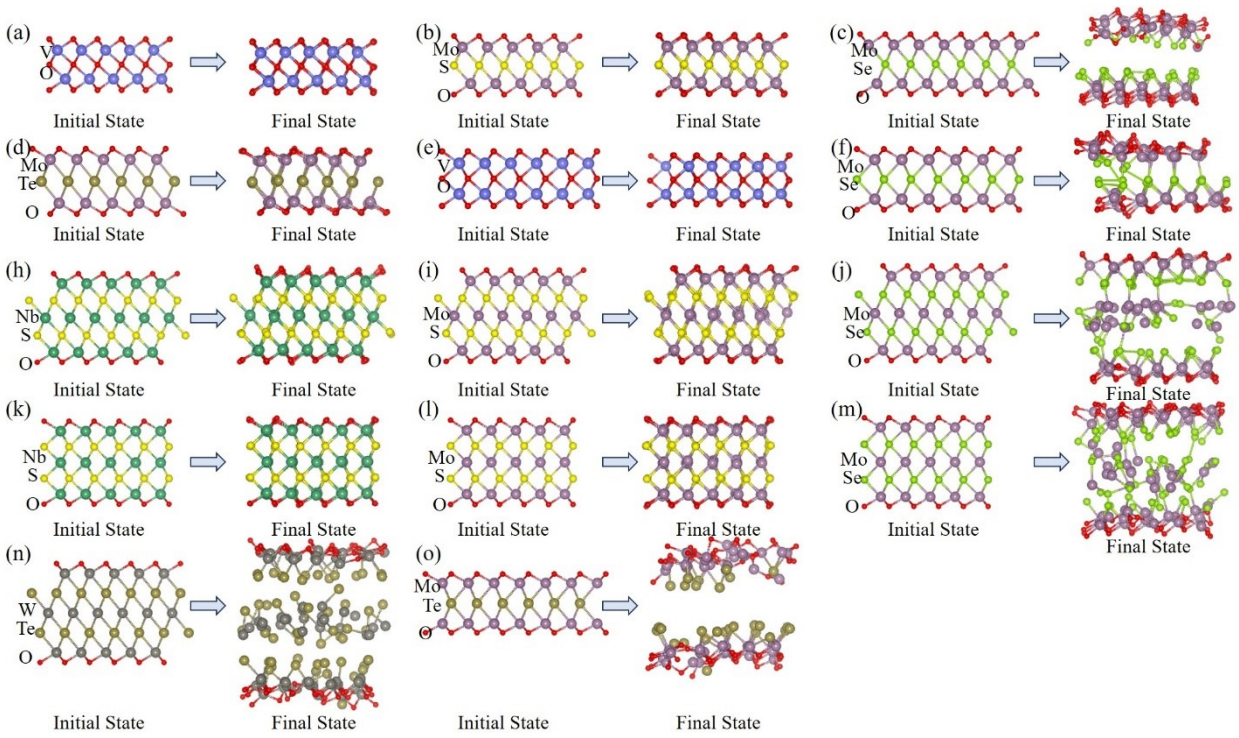

Fig. S9 Initial and final states for 14 MOenes from AIMD simulations.

Table S2 The thermodynamic competitors for 14 candidates, and the corresponding formation energy from first-principles calculations.

MOenes	Competitors	$E_{formation}$ (eV/atom)
1T-V_2O_3	V_2O_5, VO	-0.239
1T-Mo_2SO_2	MoS_2, Mo_4O_5, MoO_2	0.158
1T-Mo_2SeO_2	$MoSe_2$, Mo_4O_5, MoO_2	0.266
1T-Mo_2TeO_2	$MoTe_2$, Mo_4O_5, MoO_2	0.301
1T-$Nb_3S_2O_2$	NbS_2, NbO	0.171
1T-$Mo_3S_2O_2$	MoS_2, Mo_2O, MoO_2	-0.226
1T-$Mo_3Se_2O_2$	$MoSe_2$, Mo_2O, MoO_2	-0.085
1T-$W_3Te_2O_2$	WTe_2, W_3O, WO_2	0.207
2H-V_2O_3	V_2O_5, VO	-0.278
2H-Mo_2SeO_2	$MoSe_2$, Mo_4O_5, MoO_2	0.34
2H-Mo_2TeO_2	$MoTe_2$, Mo_4O_5, MoO_2	0.378
2H-$Nb_3S_2O_2$	NbS_2, NbO	0.171
2H-$Mo_3S_2O_2$	MoS_2, Mo_2O, MoO_2	-0.241
2H-$Mo_3Se_2O_2$	$MoSe_2$, Mo_2O, MoO_2	-0.036

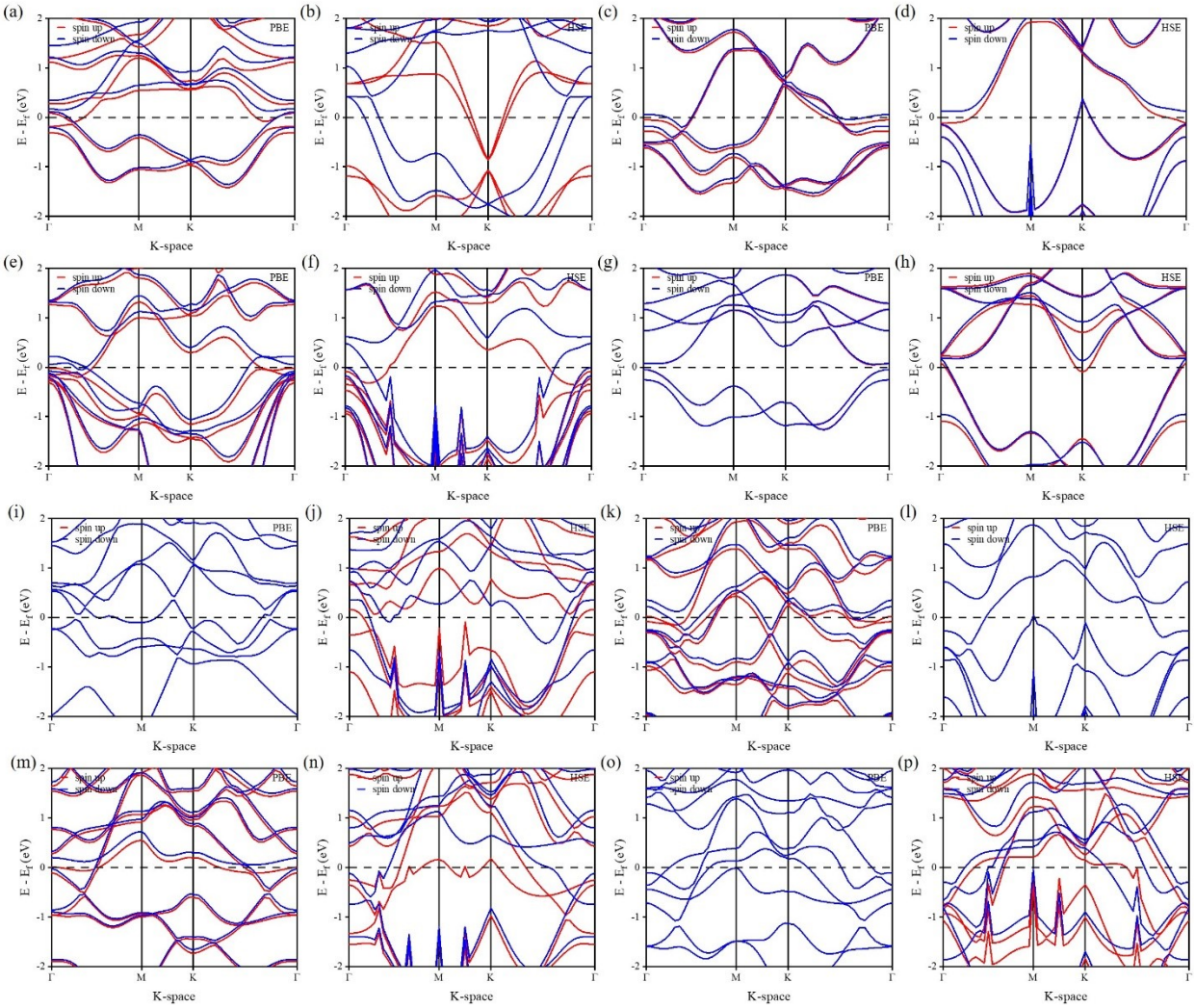

Fig. S10 Electronic band structures for 1T-V_2O_3 from (a) PBE and (b) HSE06 calculations, 1T-Mo_2SO_2 from (c) PBE and (d) HSE06 calculations, 1T-Mo_2TeO_2 from (e) PBE and (f) HSE06 calculations, 2H-V_2O_3 from (g) PBE and (h) HSE06 calculations, 1T-$Nb_3S_2O_2$ from (i) PBE and (g) HSE06 calculations, 1T-$Mo_3S_2O_2$ from (k) PBE and (l) HSE06 calculations, 2H-$Nb_3S_2O_2$ from (m) PBE and (n) HSE06 calculations, 2H-$Mo_3S_2O_2$ from (o) PBE and (p) HSE06 calculations, respectively.

References

S1 G. Kresse and J. Furthmüller, *Phys. Rev. B*, 1996, **54**, 11169-11186.

S2 P. E. Blöchl, *Phys. Rev. B*, 1994, **50**, 17953-17979.

S3 S. Grimme, J. Antony, S. Ehrlich and H. A Krieg, *J. Chem. Phys.*, 2010, **132**, 154104.

S4 J. K. Nørskov, T. Bligaard, A. Logadottir, J. R. Kitchin, J. G. Chen, S. Pandelov and U. Stimming, *J. Electrochem. Soc.*, 2005, **152**, J23-J26.

S5 K. Mathew, R. Sundararaman, K. Letchworth-Weaver, T. A. Arias and R. G. Hennig, *J. Chem. Phys.*, 2014, **140**, 084106.

S6 S. Nosé, *J. Chem. Phys.*, 1984, **81**, 511.

S7 K. Momma and F. Izumi, *J. Appl. Cryst.*, 2011, **44**, 1272–1276.

S8 J. Heyd, G. E. Scuseria and M. Ernzerhof, *J. Chem. Phys.*, 2003, **118**, 8207.